

Bifurcation and stability of uniformly rotating homogeneous ellipsoids surrounded by a massive thin ring

Shin'ichirou Yoshida*

*Department of Earth Science and Astronomy, Graduate School of Arts and Sciences, The University of Tokyo
Komaba 3-8-1, Meguro-ku, Tokyo 153-8902, Japan*

(Dated: January 25, 2023)

We examine the effects of a massive concentric ring around a spheroid or an ellipsoid with uniform density and uniform rotation. Equilibrium sequences of axisymmetric Maclaurin-like spheroid and triaxial Jacobi-like ellipsoids are obtained. Due to the gravitational field of the ring, Maclaurin-like spheroid does not have a spherical limit when the object's angular frequency vanishes. At a critical value of the eccentricity of the spheroid's meridional section, a triaxial Jacobi-like ellipsoid bifurcates. When a parameter characterizing the gravitational field of the ring is smaller than a threshold, the bifurcation points of Maclaurin-like and Jacobi-like ellipsoids exist and the critical eccentricity is slightly larger than that of the classical Maclaurin-to-Jacobi bifurcation. When the parameter exceeds the threshold, the Maclaurin-like spheroid does not have the bifurcation point and the Jacobi-like ellipsoid appears at the lower eccentricity than the Maclaurin-like spheroid. By comparisons of the energy of the ellipsoids with the same angular momentum, it is shown that the critical point of bifurcation does not correspond to the onset of the secular instability of Maclaurin-like spheroid. It is concluded that the gravitational field of a massive ring surrounding a uniformly rotating spheroid stabilizes it against a bar-shaped deformation due to viscous dissipations.

PACS numbers: 47.20.Ky, 47.32.Ef, 96.30.W, 96.30.Iz, 96.15.Ef, 98.52.Eh, 98.56.Ew

I. INTRODUCTION

Rotating equilibrium figures of self-gravitating fluid have a long history of studies since Isaac Newton's time. The studies have been motivated by the pursuits of possible configurations of planets, stars, stellar clusters, and galaxies, which span many orders of magnitude in physical sizes and timescales. The simplest and still useful models are the uniform-density and uniformly rotating spheroids and ellipsoids, which enable analytic expressions of physical characteristics (see Lyttleton 1, Chandrasekhar 2 for the classical results). These simple results are still useful in, for instance, studying the equilibrium figure of a dwarf planet, Haumea, which is thought to have a triaxial ellipsoidal shape [3–5]. In a completely different context of compact star physics, the models have been utilized to mimic the rapidly rotating compact stars, which may assume time-dependent triaxial ellipsoid. Then the objects emit gravitational waves whose frequencies are optimal for the ground-based gravitational-wave observatories [6]. For some of the recent applications of the classical ellipsoids to compact stars, see, e.g., [7–9]. At a larger scale, the classical ellipsoids are applied to model star clusters [10] or elliptical galaxies surrounded by dark matter haloes [11]. In fact, closely related studies to ours have been done by Kondratyev and his collaborators [11–13], where the effects of a circum-galactic dark matter ring on the elliptical galaxies are investigated to explain the origin of the highly flattened Early-type galaxies. An apparent lack of rota-

tional velocity in some of the highly-flattened ellipsoidal galaxies are attributed to the tidal effect of a massive concentric ring around a uniformly rotating ellipsoid.

In this paper, we use the same model as that of Kondratyev and his collaborators to study more fundamental issues of ellipsoidal figures. One of the issues is the bifurcation point of the Maclaurin-like axisymmetric spheroid (which we call M-spheroid hereafter) and the Jacobi-like triaxial ellipsoid (hereafter J-ellipsoid) under the influence of the ring's gravity. It is well-known that the classical Maclaurin spheroid with uniform density and uniform rotation has the eccentricity e of its meridional section that spans from zero to unity. An object with $e = 0$ corresponds to a non-rotating object, while $e = 1$ corresponds to an infinitely thin disk. For $e \geq 0.81267$, there exists another triaxial ellipsoid with uniform rotation and with the same angular momentum as Maclaurin spheroid, which is called Jacobi ellipsoid [1, 2]. It is not known how this classical picture is modified when the spheroid/ellipsoid is surrounded by a massive ring. Do we always have a bifurcation point of the axisymmetric M-spheroid and the triaxial J-ellipsoid for any parameter choice of the massive ring? Another issue is the secular stability of the M-spheroids. Beyond the bifurcation point ($e = 0.81267$), the classical Maclaurin spheroid has a larger energy than the Jacobi ellipsoid with the same angular momentum. When viscous dissipation is taken into account, the Maclaurin spheroid becomes secularly unstable and evolves towards the Jacobi ellipsoid by preserving the angular momentum [14, 15]. When the tidal field of the massive ring surrounding the spheroid/ellipsoid, do we expect the same secular instability for the axisymmetric configuration beyond the corresponding bifurcation point?

*Electronic address: yoshida@ea.c.u-tokyo.ac.jp

Although these issues may appear academic at first sight, they are related to the structure and the stability of various astrophysical objects. For instance, they are relevant to the formation and stability of rapidly rotating dwarf planets with rings. A newly born proto-neutron star or a strange star after the iron-core collapse of a dying massive star or a massive remnant neutron star of a neutron-star binary merger may rotate rapidly enough to be secularly unstable to viscous dissipation. These may be potential sources of quasi-monochromatic gravitational waves which are detectable by the network of ground-based gravitational wave observatories. When they are surrounded by a massive torus of fallback matter or of merger debris, how does this picture change? If the dark matter distribution around some of the elliptical galaxies or around the bulges of spiral galaxies may be mimicked by that of the ring (as is suggested by Kondratyev et al. 13), do we expect to see the stellar systems as spheroids or triaxial ellipsoids? These questions of completely different scales in the Universe may be related to the simple models considered here.

II. MODELS

In the theory of homogeneous ellipsoidal figures [1, 2], the isobaric surfaces are assumed to form concentric ellipsoids and the surface at which the pressure vanishes is parametrized with the semi-major axes a_1, a_2, a_3 , thus the surface is defined as

$$\frac{x^2}{a_1^2} + \frac{y^2}{a_2^2} + \frac{z^2}{a_3^2} = 1. \quad (1)$$

Here we employ a Cartesian coordinate (x, y, z) whose origin is at the center of mass and the coordinate axes are along the semi-major axes. Without loss of generality, we may assume $a_3 \leq a_2 \leq a_1$ for the oblate cases we are interested in here.

A. Ring potential

The gravitational potential of a thin ring of mass m_o and radius R_o , which is a solution of a Poisson's equation, is given as a series [16],

$$\Phi_o = -Gm_o \sum_{n=0}^{\infty} \frac{(4n-1)!!}{2^{2n}(n!)^2} \frac{(RR_o)^{2n}}{(R^2 + R_o^2 + z^2)^{2n+\frac{1}{2}}}, \quad (2)$$

where the cylindrical coordinate (R, z) is used whose z -axis coincides with the rotational axis of the ellipsoid. To make the solutions semi-analytic, we truncate the ring potential at the quadratic order in R and z , thus $n = 0, 1$ in the series. Then the ring potential is approximated as

$$\Phi_o = -\frac{Gm_o}{R_o} \left[1 + \frac{1}{4} \left(\frac{R}{R_o} \right)^2 - \frac{1}{2} \left(\frac{z}{R_o} \right)^2 \right]. \quad (3)$$

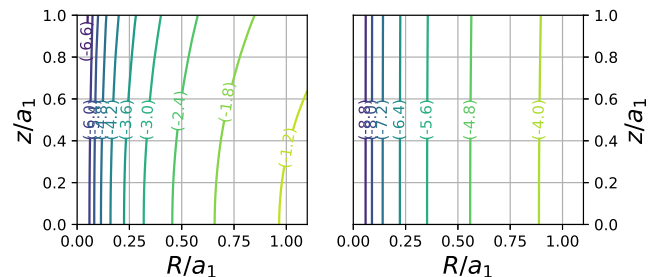


FIG. 1: Truncation error of the series expansion of the ring potential (Eq.2) at $n = 1$. The contours of the logarithm of the ratio $\frac{\sum_{n=2}^N \phi_n}{\sum_{n=0}^N \phi_n}$ are shown in the (R, z) -plane. ϕ_n is the n -th term of Eq.(2). The left panel is for $R_o/a_1 = 2$ and the right one is for $R_o/a_1 = 10$.

The same expression is obtained by [12] by a-priori assumption of the quadratic form. In Fig.1, the truncation error of Eq.(2) is shown as contour plots in (R, z) -plane. The error is estimated as

$$\text{error} = \frac{\sum_{n=2}^N \phi_n}{\sum_{n=0}^N \phi_n}, \quad \phi_n \equiv \frac{(4n-1)!!}{2^{2n}(n!)^2} \frac{(RR_o)^{2n}}{(R^2 + R_o^2 + z^2)^{2n+\frac{1}{2}}}, \quad (4)$$

where N is a sufficiently large integer. We adopt $N = 50$ here. The coordinate is normalized by the longest semi-major axis a_1 and the logarithm of the error is shown here. In an ellipsoid ($0 \leq R/a_1, z/a_1 \leq 1$), the error is largest at the equatorial surface. For $R_o/a_1 = 2$, the largest error amounts to a few percent, while the largest error is less than 10^{-3} percent for $R_o/a_1 = 10$. As is expected, the truncation gives the better approximation for the larger R_o .

B. Ellipsoidal equations

The hydrostatic equation of stationary configuration rotating with the angular frequency Ω reads

$$\frac{1}{\rho} \frac{\partial}{\partial x_j} p = -\frac{\partial}{\partial x_j} \Phi + x_j \Omega^2 (1 - \delta_{j3}) \quad j = 1, 2, 3, \quad (5)$$

where $x_1 = x, x_2 = y, x_3 = z$. Φ is the total gravitational potential. The first integral form of the equation is

$$\frac{p}{\rho} = -\Phi + \frac{1}{2} (x^2 + y^2) \Omega^2 + C, \quad (6)$$

where C is a constant.

The internal potential Φ_i of the self-gravitating uniform density ellipsoid is expressed by a simple quadratic

form

$$\Phi_i = -\pi G\rho [A - A_1x^2 - A_2y^2 - A_3z^2]. \quad (7)$$

The coefficients A_j are given by

$$A_j = a_1a_2a_3 \int_0^\infty \frac{du}{(a_j^2 + u)\Delta}, \quad A = \sum_{j=1}^3 a_j^2 A_j, \quad (8)$$

where $\Delta^2 = (a_1^2 + u)(a_2^2 + u)(a_3^2 + u)$.

Since the potential of the ring mass is given by Eq.(3), the total potential $\Phi = \Phi_i + \Phi_o$ is written as

$$\begin{aligned} \Phi &= -\frac{3GM}{4a_1a_2a_3} \left[A + \frac{4a_2a_3m_o}{3\lambda M} \right. \\ &\quad - \left(A_1 - \frac{a_2a_3m_o}{3\lambda^3a_1^2M} \right) x^2 - \left(A_2 - \frac{a_2a_3m_o}{3\lambda^3a_1^2M} \right) y^2 \\ &\quad \left. - \left(A_3 + \frac{2a_2a_3m_o}{3\lambda^3a_1^2M} \right) z^2 \right] \\ &\equiv -\frac{3GM}{4a_1a_2a_3} [A' - A_1'x^2 - A_2'y^2 - A_3'z^2]. \quad (9) \end{aligned}$$

Here $\lambda = R_o/a_1$.

From the condition that the surface of the ellipsoid coincides with the equipotential surface, we have

$$a_1^2 \left(A_1' - \frac{\Omega^2}{2\pi G\rho} \right) = a_2^2 \left(A_2' - \frac{\Omega^2}{2\pi G\rho} \right) = a_3^2 A_3'. \quad (10)$$

Then the equalities,

$$a_1^2 a_2^2 (A_1' - A_2') + (a_1^2 - a_2^2) a_3^2 A_3' = 0 \quad (11)$$

and

$$\frac{\Omega^2}{2\pi G\rho} = \frac{a_1^2 A_1' - a_2^2 A_2'}{a_1^2 - a_2^2} = \frac{a_1^2 A_1' - a_3^2 A_3'}{a_1^2} = \frac{a_2^2 A_2' - a_3^2 A_3'}{a_2^2}, \quad (12)$$

hold. From the definition of A_i 's and A_i' 's above, we may deduce from Eq.(11) that

$$\begin{aligned} (a_2^2 - a_1^2) \left[\int_0^\infty \left(\frac{a_1^2 a_2^2}{(a_1^2 + u)(a_2^2 + u)} - \frac{a_3^2}{a_3^2 + u} \right) \frac{du}{\Delta} \right. \\ \left. - \frac{2}{3} \lambda^{-3} \frac{m_o}{M} \left(\frac{a_3}{a_1} \right)^2 \right] = 0 \quad (13) \end{aligned}$$

This equation results in two equilibrium sequences. One is the case that $a_1 = a_2$ holds. This corresponds to axisymmetric spheroids. We call them M-spheroid sequence. The other is when the expression in the square bracket vanishes. It corresponds to sequences of non-axisymmetric triaxial ellipsoids. We call them J-ellipsoids. The functional relation of Ω and the normalized principal axes for an M-spheroid sequence is given by the second or third equality of Eq.(12). For a J-ellipsoid sequence, the expression in the square bracket of Eq.(13) is set zero and solved for a_3 when a_1 and a_2 is specified. The values of a_j 's are substituted to Eq.(12) to

obtain Ω . The bifurcation point of M-spheroid and J-ellipsoid sequences corresponds to the special solution of this equation for J-ellipsoid by setting $a_1 = a_2$.

Following the conventional treatment of the ellipsoidal figures, we parametrize the sequences by the eccentricity e of the meridional section of the ellipsoids,

$$e = \sqrt{1 - \left(\frac{a_3}{a_1} \right)^2}. \quad (14)$$

C. Expressions of energy and Angular momentum

The rotational kinetic energy T of a uniformly rotating ellipsoid is obtained by

$$T = \frac{1}{2} I_z \Omega^2, \quad (15)$$

where I_z is the moment of inertia and is computed by

$$I_z = \frac{4}{15} \pi \rho a_1 a_2 a_3 (a_1^2 + a_2^2). \quad (16)$$

The angular momentum J is simply given by $J = I_z \Omega$.

The gravitational energy W is given by,

$$W = W_i + W_o = \frac{1}{2} \int \rho \Phi_i dV + \int \rho \Phi_o dV. \quad (17)$$

Notice that the potential Φ_i is produced by the mass of the ellipsoid itself, thus the contribution from the self-gravity is multiplied by the 1/2 factor to cancel the double count, while Φ_o is the external potential created by the ring, which does not require the factor. The self-gravity term W_i is computed as,

$$W_i = -\frac{8}{15} \pi^2 G \rho a_1 a_2 a_3 A, \quad (18)$$

while the ring contribution is,

$$W_o = -\frac{Gm_o}{R_o} \frac{4\pi\rho}{3} a_1 a_2 a_3 \left[1 + \frac{1}{20} \frac{a_1^2 + a_2^2}{R_o^2} - \frac{1}{10} \frac{a_3^2}{R_o^2} \right]. \quad (19)$$

The total energy of an ellipsoid is $E = T + W$.

D. Numerical treatment

To obtain the functional relation of Ω and the principal axes of the ellipsoid, we need to evaluate elliptic integrals appearing in A_j 's. More specifically, the integral we use has the form,

$$R_J(x, y, z, p) = \frac{3}{2} \int_0^\infty \frac{du}{(u+p) \sqrt{(u+x)(u+y)(u+z)}}. \quad (20)$$

This is one of Carlson's elliptic integrals [17, 18]. We use a `python` version of TOMS577 library to compute this integral. [21]

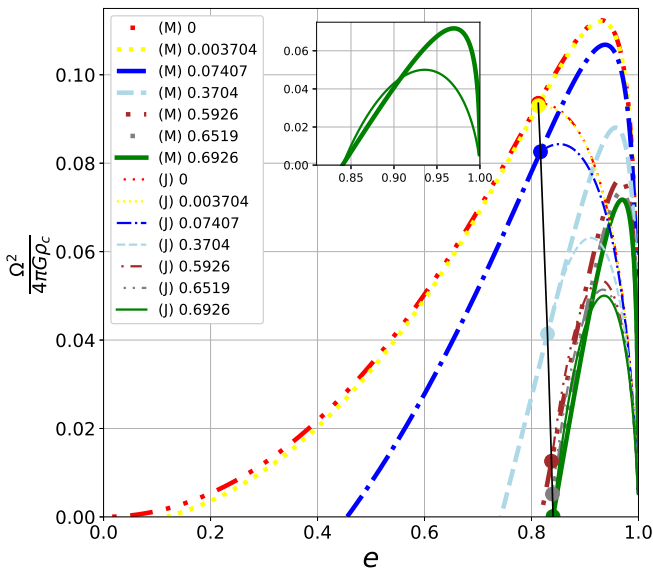


FIG. 2: The angular frequency squared Ω^2 , normalized by $4\pi G\rho_c$, is plotted as a function of the eccentricity $e = \sqrt{1 - (a_3/a_1)^2}$. The averaged axis \bar{a} is defined as $\bar{a} = (a_1 a_2 a_3)^{1/3}$. The thick curves with a label (M) are M-spheroids, while those with (J) are J-ellipsoids. The number in the legend is the value of ν , where $\nu = 0$ curves are the original Maclaurin and the Jacobi sequences. The filled circles and the solid curve connecting them mark the bifurcation points of M-spheroids and J-ellipsoids. The inset shows the M-spheroids and the J-ellipsoids sequences of $\nu = 0.6926$, for which $\Omega = 0$ at the bifurcation.

III. RESULTS

A. Angular frequency

As is seen in Eq.(9),(12),(13), the sequences of Ω^2 as a function of the eccentricity e are characterized by the dimensionless parameter $\nu \equiv \lambda^{-3} m_o/M$. From the expression of the parameter,

$$\nu = \lambda^{-3} \frac{m_o}{M} = \left(\frac{R_o}{a_1}\right)^{-3} \frac{m_o}{M} = \frac{G m_o a_1^2}{R_o^3 G M} \sim \frac{\Phi_o(a_1)}{\Phi_i(a_1)}, \quad (21)$$

its physical significance is the relative strength of the ring's gravitational field compared with that of the ellipsoid at the surface.

In Fig.2, sequences of Ω^2 for the M-spheroids and the J-ellipsoids are plotted as functions of eccentricity. For a given line style, the thicker curve corresponds to the M-spheroid sequence. The bifurcation points for each ν are marked with the circles. We see that the normalized frequency decreases as the parameter ν increases. Also, the M-spheroid sequence in general does not have a $e \rightarrow 0$ limit. This is in accord with the result by [13], and in contrast to the Maclaurin spheroid embedded in a massive spherical halo [19], for which the sequences always seem to extend to $e \rightarrow 0$.

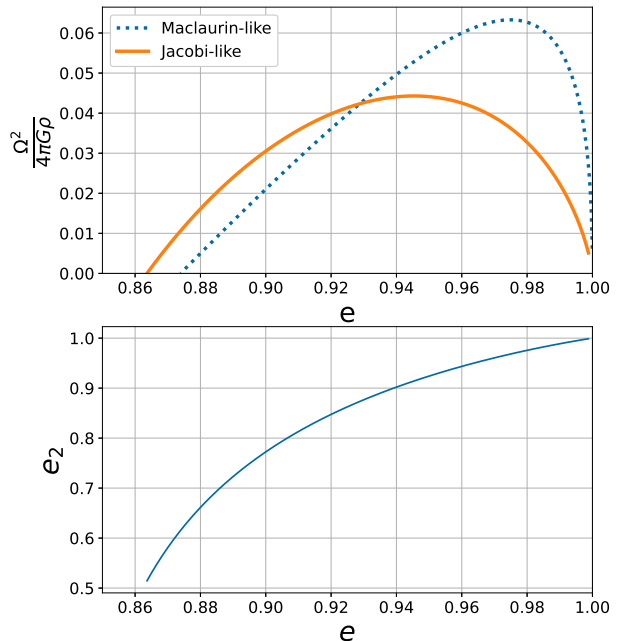


FIG. 3: Top: An M-spheroid and a J-ellipsoid sequence for $\nu > 0.6926$. Here $m_o = 3$ and $\lambda = 1.5$, thus $\nu = 0.8889$. Bottom: The eccentricity e in the x-z-section versus that of the x-y-section e_2 for the J-ellipsoid sequence above.

For a small value of ν (≤ 0.3108), the Jacobi-like model always has a lower Ω than the M-spheroid model with the same e . As ν increases, however, there appears a range of e within which Ω of J-ellipsoids becomes larger than that of M-spheroids. This is clearly seen in the inset.

As ν increases, the normalized Ω^2 decreases, though the eccentricity at the bifurcation changes little. Overall, the eccentricity of the bifurcation point shifts at most 3.4%. This is compared with the result by [20] who showed the bifurcation point of the Maclaurin spheroid embedded in a concentric spheroidal halo shifts more than 10% as the density of the halo doubles the central spheroid.

Another remarkable trait of the bifurcation is that for $\nu > 0.6926$, the bifurcation point vanishes at which an M-spheroid and a J-ellipsoid coincide. For this case, shown in Fig.3, a J-ellipsoid appears at a lower eccentricity than an M-spheroid, and the former can be a configuration with zero rotational frequency. The intersection of the two curves is not a bifurcation point of the M-spheroid and the J-ellipsoid sequences. This is seen in the lower panel of Fig.3, where the eccentricities of the J-ellipsoids in x-z- and x-y-sections are compared. The eccentricity in the x-y-section, e_2 , is defined as $e_2 = \sqrt{1 - (a_2/a_1)^2}$. For a M-spheroid, $e_2 = 0$ by definition. Therefore the two sequences do not share the e_2 value at the intersec-

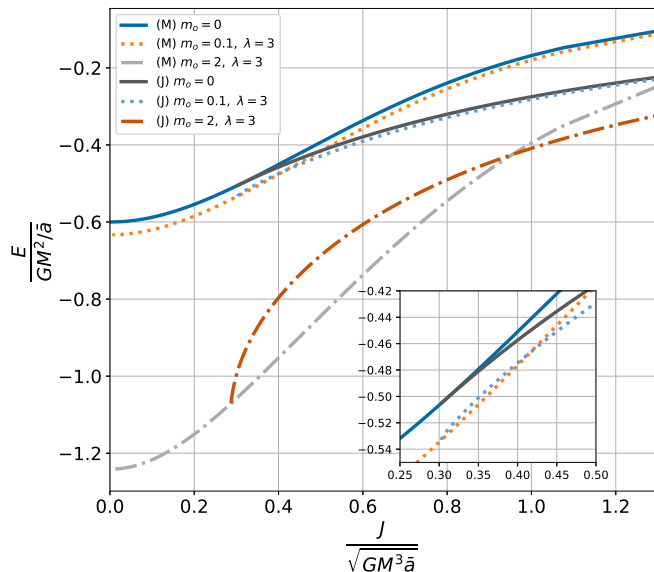


FIG. 4: The energy as a function of the angular momentum of the ellipsoids. The energy E is normalized by GM^2/\bar{a} and the angular momentum is normalized by $\sqrt{GM^3\bar{a}}$. The inset shows the enlarged picture around the bifurcation points for $m_o = 0$ and 0.1 models.

tion point of the two curves, though the two sequences of ellipsoids would have shared it at a genuine bifurcation point.

B. Secular stability of M-spheroid

Notice that the parameters λ and m_o/M are not degenerate in the expression of the energy (see Eq.(19)), thus the models are not represented by the single parameter ν , but we need to specify both m_o/M and λ . In Fig.4, we plot the energy as a function of the angular momentum for the M-spheroid and the J-ellipsoid sequences. The parameters are chosen so that $\nu < 0.6926$. The enlarged view of the sequences around the bifurcation points are shown in the inset. The original Maclaurin spheroid always has a higher energy than the Jacobi ellipsoid with the same angular momentum. Therefore the Maclaurin spheroids are secularly unstable beyond the bifurcation point. Viscous energy dissipation would drive the Maclaurin spheroid to the lower-energy Jacobi ellipsoid with the same angular momentum. When the gravitational field of the ring is turned on, the J-ellipsoid may have higher energy than the M-spheroid around the bifurcation point. The energy of the former becomes lower than the latter for sufficiently large angular momentum. Thus the M-spheroid is secularly stable at least around the bifurcation point and the neutral stability point is located at a higher angular momentum. For the case with $\nu > 0.6926$, the J-ellipsoid sequence always has larger energy than the M-spheroid sequence. Thus the tidal field of the massive ring stabilizes the M-spheroids against the

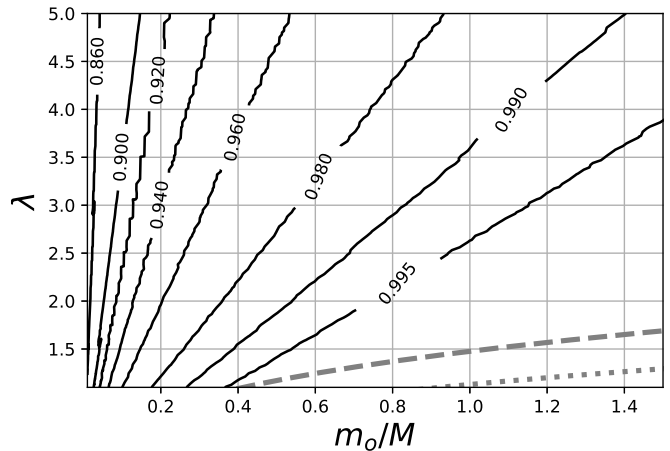


FIG. 5: Contour map of the eccentricity of M-spheroids at their neutral stability. The dashed line is the curve with $\nu = 0.3108$, while the dotted line is for $\nu = 0.6926$.

bar-shaped bifurcation to triaxial ellipsoids.

In Fig.5, the eccentricity e of the M-spheroid at which its total energy equals that of the J-ellipsoid with the same angular momentum (it should be noted that the ellipsoid does not necessarily share the eccentricity with the M-spheroid). Below a contour curve, the M-spheroid with the eccentricity lower than the labeled value is secularly unstable to viscous dissipation, since its energy is higher than the J-ellipsoid. It should be noted that the classical Maclaurin spheroid becomes secularly unstable for $e \geq 0.81267$. The gravity of the ring makes the M-spheroid more stable and the effect is enhanced as $\nu = \lambda^{-3}m_o/M$ becomes larger (towards the bottom right corner of the figure).

IV. SUMMARY AND DISCUSSION

We studied the uniformly rotating homogeneous ellipsoidal sequences under the influence of the gravitational field of a massive concentric ring. The ring potential is truncated at the quadrupole term in order for the study to be semi-analytic. The resulting expressions for the various physical quantities have correction terms determined by the mass and the radius of the ring. When the mass is reduced to zero or the radius is set to be infinite, we recover the classical Maclaurin spheroids and the Jacobi ellipsoids. The existence of the massive ring modifies the bifurcation and the secular stability of the ellipsoids. The meridional section of an M-spheroid with zero angular frequency has a finite eccentricity e due to the gravitational attraction of the ring mass. Thus the sequence is not extended to $e = 0$ limit. If the parameter ν which measures the gravitational field of the ring is smaller than $\nu = 0.6926$, a J-ellipsoid bifurcates from an M-spheroid at some value of e as is seen in the classical Maclaurin sequence. Beyond this threshold, the bifurcation point vanishes, and the J-ellipsoid exists at a lower e than the

M-spheroid appears. Examining the total energy of the M-spheroid and the J-ellipsoid with the same angular momentum, the M-spheroid is not secularly unstable to viscous dissipation around the bifurcation point, in contrast to the classical Maclaurin spheroid which is destabilized beyond the bifurcation point of Jacobi ellipsoids. When parametrized by the eccentricity, the stabilization occurs before the rotational frequency of the J-ellipsoid may exceed that of the M-ellipsoid ($\nu \leq 0.3108$).

It may seem counter-intuitive that a non-rotating object with an external axisymmetric ring source develops

a triaxial shape as is seen in Fig.4. This occurs when the gravity of the ring is comparable to the self-gravity of the ellipsoid ($\nu > 0.6926$). On the equatorial plane ($z = 0$), the ring's potential (Eq.2) is quadratic in the cylindrical radial coordinate. Therefore it may be effectively identified as the rotational term in Eq.(6). In other words, the gravitational attractive force of the circum-object ring induces an effective centrifugal effect on the ellipsoid. It results in the appearance of the Jacobi-like triaxial ellipsoid even if the object's rotational frequency vanishes.

-
- [1] R. A. Lyttleton, *The stability of rotating liquid masses* (Cambridge University Press, Cambridge, 1953).
- [2] S. Chandrasekhar, *Ellipsoidal figures of equilibrium* (Dover, New York, 1987).
- [3] J. L. Ortiz, et al., *Nature* **550**, 219 (2017), 2006.03113.
- [4] E. T. Dunham, S. J. Desch, and L. Probst, *The Astrophysical Journal* **877**, 41 (2019), URL <https://dx.doi.org/10.3847/1538-4357/ab13b3>.
- [5] J. L. Noviello, S. J. Desch, M. Neveu, B. C. N. Proudfoot, and S. Sonnett, *Planetary Sci. J.* **3**, 225 (2022).
- [6] B. P. Abbott et al., *Living Rev. Relativity* **23**, 3 (2020).
- [7] P. B. Rau and A. Sedrakian, *Mon. Not. Roy. Astron. Soc.* **509**, 1854 (2022), 2108.02881.
- [8] G. Yim and D. I. Jones, *Mon. Not. Roy. Astron. Soc.* **511**, 1942 (2022), 2109.05076.
- [9] J. A. Rueda, R. Ruffini, L. Li, R. Moradi, J. F. Rodriguez, and Y. Wang, *Phys. Rev. D* **106**, 083004 (2022), 2203.16876.
- [10] P. B. Ivanov and D. N. C. Lin, *Astrophys. J.* **904**, 171 (2020), 2009.13467.
- [11] B. P. Kondratyev, N. G. Trubitsyna, and E. N. Kireeva, *Baltic Astronomy* **24**, 408 (2015).
- [12] B. P. Kondratyev and N. G. Trubitsyna, *Astrophysics* **53**, 189 (2010).
- [13] B. P. Kondratyev, N. G. Trubitsyna, and E. N. Kireeva, *Astronomy Reports* **60**, 526 (2016).
- [14] P. H. Roberts and K. Stewartson, *Astrophys. J.* **137**, 777 (1963).
- [15] W. H. Press and S. A. Teukolsky, *Astrophys. J.* **181**, 513 (1973).
- [16] J. Selvaggi, S. Salon, and M. V. K. Chari, *Am. J. Phys.* **75**, 724 (2007).
- [17] B. Carlson, *Numer. Math.* **33**, 1 (1979).
- [18] B. Carlson and N. E., *ACM Trans. Math. Software* **7**, 398 (1981).
- [19] H. Robe and L. Leruth, *Astron. & Astrophys.* **133**, 369 (1984).
- [20] M. Miyamoto, *Publ. Astron. Soc. Japan* **19**, 242 (1967).
- [21] https://people.math.sc.edu/Burkardt/py_src/toms577/toms577.